Journal of Power Sources 194 (2009) 243–251

Contents lists available at ScienceDirect

Journal of Power Sources

journal homepage: www.elsevier.com/locate/jpowsour

Study of different nanostructured carbon supports for fuel cell catalysts

Daniele Mirabile Gattia[a,*], Marco Vittori Antisari[a], Leonardo Giorgi[a], Renzo Marazzi[a], Emanuela Piscopiello[b], Amelia Montone[a], Serafina Bellitto[c], Silvia Licoccia[c], Enrico Traversa[c]

[a] Department of Physical Methods and Materials, ENEA, Research Centre of Casaccia, Via Anguillarese 301, 00123 Rome, Italy
[b] Department of Physical Methods and Materials, ENEA, Research Centre of Brindisi, Via Appia Km 702, 72100 Brindisi, Italy
[c] Dipartimento di Scienze e Tecnologie Chimiche, Università di Roma "Tor Vergata", Via della Ricerca Scientifica, 00133 Rome, Italy

ARTICLE INFO

Article history:
Received 20 January 2009
Received in revised form 31 March 2009
Accepted 23 April 2009
Available online 3 May 2009

Keywords:
Carbon nanostructures
Catalyst
Fuel cell
Methanol
Electro-catalytic activity

ABSTRACT

Pt clusters were deposited by an impregnation process on three carbon supports: multi-wall carbon nanotubes (MWNT), single-wall carbon nanohorns (SWNH), and Vulcan XC-72 carbon black to investigate the effect of the carbon support structure on the possibility of reducing Pt loading on electrodes for direct methanol (DMFC) fuel cells without impairing performance. MWNT and SWNH were in-house synthesised by a DC and an AC arc discharge process between pure graphite electrodes, respectively. UV–vis spectrophotometry, scanning and transmission electron microscopy, X-ray diffraction, and cyclic voltammetry measurements were used to characterize the Pt particles deposited on the three carbon supports. A differential yield for Pt deposition, not strictly related to the surface area of the carbon support, was observed. SWNH showed the highest surface chemical activity toward Pt deposition. Pt deposited in different forms depending on the carbon support. Electrochemical characterizations showed that the Pt nanostructures deposited on MWNT are particularly efficient in the methanol oxidation reaction.

1. Introduction

Direct methanol (DMFC) fuel cells have demonstrated to be suitable technologies for automotive and low power portable electronic device applications due to their high power density and low working temperatures. One of the main problems that hinder a large diffusion of DMFCs is the use in the electrodes of expensive noble metals, Pt and Ru, as single particles or alloys. Reduction of the Pt content can conceptually be obtained following two ways: (1) increasing Pt utilization, and (2) substituting Pt with other elements with appropriate catalytic properties toward the anodic and cathodic reactions. Pt alloys with Ru [1], Ni, Cr, Co [2,3], as well as other ternary [4] and quaternary [5] alloys have been studied but the stability and activity of these alloys after long time operation need to be verified. Enhanced catalyst utilization could be obtained by increasing the contact between the catalyst, the proton conductive polymer, and the reactants. This could be achieved either via optimization of the membrane-electrode assembly (MEA), or by using for the catalyst a support with tailored microstructural, surface chemical and electronic properties. Moreover, physical and chemical properties of the carbon support also influence the yield for catalyst deposition, which has to be taken into account to estimate the cost for the electrode preparation, and consequently the cost of fuel cells.

The interaction of the platinum precursor with the support during the deposition process varies with surface heterogeneities and structural features of carbon support, thus leading to Pt particles with different characteristics (crystallite size, lattice parameters, and amorphous content [6,7]) and with dissimilar anchoring strength to the support itself [8,9]. The carbon material structure can play an important role in the catalyst dispersion, in its crystallographic characteristics, and consequently in its electrochemical properties [10–13] and in the way the catalyst redistributes on the carbon support surface during cell operation.

The use of carbon nanotubes, discovered in 1991 [14], for fuel cell applications has been recently experimented and largely reviewed [15]. The higher accessibility of catalysts deposited on nanotubes is supposed to favour catalyst utilization [16]. Better performance of carbon nanotube-based electrodes with respect to carbon black-based electrodes has also been correlated to the higher electronic conductivity of the former (10^4 S cm^{-1} [17]) with respect to the latter (4.0 S cm^{-1}, in the case of Vulcan XC-72 [18]) [19]. Non-catalyzed and catalyzed oxidations of MWNT have been reported by Li et al. to evaluate their electrochemical durability as catalyst support. The comparison with carbon black Vulcan XC-72 demonstrated that MWNT are more resistant to electrochemical oxidation [20]. Yoshitake et al. [21] showed how fuel cell performance could be enhanced if single walled carbon nanohorns (SWNH), first reported in [22], were used as Pt support.

* Corresponding author. Tel.: +39 06 30483484.
E-mail address: daniele.mirabile@enea.it (D. Mirabile Gattia).

0378-7753/$ – see front matter © 2009 Elsevier B.V. All rights reserved.
doi:10.1016/j.jpowsour.2009.04.058

Other carbon nanostructures, in particular graphite nanofibers, have been largely studied as suitable support for catalyst [23–28]. In particular, Bessel et al. [29] reported about the deposition of Pt on various types of nanofibers and their electrochemical activity in the oxidation of methanol reaction was studied. The authors ascribed the enhanced performance of these composites with respect to carbon black/Pt composite to a specific crystallographic orientation of the metal particles when deposited on highly tailored graphite nanofibers.

Therefore, literature results confirm that the use of carbon nanostructures different from carbon black is quite promising to prepare electrodes for fuel cells, both anode and cathode.

This work reports on electroless chemical deposition of Pt nanoparticles on different pure carbon nanostructures. The aim is to perform a comparison between electrodes, prepared with these composites, on the basis of microstructural and electrochemical investigations, in particular trying to discern the effect of the different carbon supports rather than studying the role of other catalysts (for example Ru). The yield for catalyst deposition on the carbon-based supports was evaluated by spectrophotometry. Microstructural characterization was performed by X-ray diffraction analysis and electron microscopy observations. Cyclic voltammetry measurements were performed to study the electrochemical surface area, the activity of the electrodes toward methanol oxidation reaction (MOR), and their ageing. Electrochemical results were correlated with the structural features of the carbon supports.

The organization of the Pt particles before and after cycling in working conditions was also investigated by analyzing the electrochemical active surface loss and mass specific activity toward methanol oxidation during cycling.

2. Experimental

2.1. Carbon materials

Multi-wall carbon nanotubes (MWNT) were synthesised with a DC arc discharge in water, as previously reported [30]. Single-wall carbon nanohorns were synthesised with an AC arc discharge in open air with the aid of a stainless steel collector, as reported elsewhere [31]. No catalysts were used to synthesise these carbon nanostructures and the investigation of "pure" platinum/carbon composites can be performed without further experimental variables introduced by other elements that could interact in the electrochemical measurements.

Vulcan XC-72 and a commercial powder containing platinum (10 wt%) deposited on Vulcan XC-72 (Pt/VU-COMM) were purchased from Cabot Corporation and E-TEK, respectively.

Table 1 summarizes the main characteristics of the carbon structures.

2.2. Pt deposition and electrode preparation

Pt deposition was carried out on different carbon supports. Three composite catalysts were prepared: (1) Pt/SWNH, (2) Pt/MWNT, and (3) Pt/VU, obtained by deposition of Pt particles on single-wall nanohorns, multi-wall carbon nanotubes, and Vulcan XC-72 carbon black, respectively. The samples were prepared with the same impregnation method. Reduction of Pt salts was achieved by using formaldehyde [34]. An adequate amount of Pt precursor was used for the Pt deposition to obtain powders with 20 wt% of Pt. The electrodes were prepared with a paint method. For the catalyst layer, slurry of Pt/C powder and ethanol was mixed with 5 wt% Nafion solution. The mixture was stirred overnight to obtain the catalyst paint. This paint was then spread on a 5 cm side square of carbon cloth on top of the gas diffusion layer, prepared with a similar paint made of carbon black and 10 wt% Teflon solution. The electrodes were dried and hot pressed. After deposition, the materials were washed with deionized water and dried at 50 °C overnight. The electrodes were prepared with a platinum loading $L_{Pt} \approx 0.5\ mg\ cm^{-2}$.

2.3. Determination of Pt content

The Pt content of the prepared composites was measured with a single ray UV–vis spectrophotometer (Beckman DU 65). The procedure was based on the Pt dissolution in aqua regia, followed by the addition of stannous chloride ($SnCl_2$) [35] and platinum–tin complex formation. The Pt content was evaluated by measuring the absorbance of the stannous chloride complex at $\lambda = 409$ nm.

The dissolution of Pt deposited on carbon in aqua regia was confirmed by EDS analysis on treated powders.

2.4. X-Ray diffraction analysis

Pt particles deposited were characterized by X-ray diffraction (XRD) analysis with a Philips X-Pert X-ray Diffractometer, with a Cu Kα source radiation and a graphite monochromator on the diffracted beam. Instrumental parameters were: divergence and scatter slits = 1°, receiving slit = 0.1 mm, voltage applied to the X-ray tube = 40 kV, electric current = 40 mA. The $20^\circ \leq 2\theta \leq 85^\circ$ range was studied with a scan step size of 0.02° and a fixed counting time of 1 s, while the (220) reflection of Pt (62–72° 2θ) was studied with a scan step size of 0.02° and a scan step time of 3 s. Warren's correction for instrumental broadening was performed [36].

The diffraction pattern of the commercial Vulcan XC-72-supported Pt catalyst was used as a comparison. X'Pert Data Collector program was used for data collection.

2.5. Morphological characterization

Powder morphology was investigated by scanning electron microscopy (SEM, LEO 1525). The samples for the SEM investigations were prepared dropping a small quantity of material, dispersed in ethanol by ultrasounds, on graphite covered aluminium stubs. Moreover, the electrodes were studied before and after cyclic voltammetry measurements.

Transmission electron microscopy (TEM, FEI TECHNAI G^2 30F) was used to investigate the Pt particles deposited on the three carbon supports. The samples were prepared as for SEM observations, expect for the use of a thin copper grid holder covered by a conductive layer of amorphous carbon.

2.6. Electrochemical characterization

Electrochemical measurements were performed at 30 °C in a standard three electrode glass cell. The electrode was inserted in a PTFE holder to be suspended in the cell. The exposed area was 0.79 cm^2. The counter electrode was a high purity graphite electrode. A calomel electrode (Hg/Hg_2Cl_2) was used as reference electrode (+0.242 V vs hydrogen normal electrode). The measurements were carried out with a PAR EG&G 273A potentiostat–galvanostat, controlled by the software CORWARE of Scribner Inc.

Two types of characterizations were carried out by cyclic voltammetry:

a) Adsorption/desorption of hydrogen on Pt particle surface to evaluate their electrochemical active surface (EAS), in a 1 M H_2SO_4

Table 1
Characteristics of the carbon nanostructures used to prepare the electrodes.

	MWNT	SWNH	Vulcan XC-72
Type of structure	Tubular structure with hollow core and closed tips	Quite-spherical particles with horn protruding from the surface, forming chains	Quite-spherical particles with smooth surface, forming chains
Diameter (nm)	10–50	20–120	20–50
Length (μm)	0.1–100	–	–
Content (%)	~80[a]	–	–
Impurities[b]	–	–	*S*
Surface area (m^2/g)	84 [32]	310 [33]	250

[a] The remaining part of the sample is represented by onion-like carbon structures.
[b] Impurities revealed by EDS analysis.

solution. EAS was measured taking into account the potential sweep at the steady state (after 50 cycles).
b) Electro-catalytic activity of the Pt particles toward methanol oxidation reaction, in a 1 M H_2SO_4 + 0.5 M CH_3OH solution.

The glass cell was purged with nitrogen gas before electrochemical measurements, to remove dissolved gaseous oxygen, and nitrogen gas was fluxed over the solution during the experiments.

Cyclic voltammetry measurements were performed between −0.3 and 1.4 V with a scanning rate of 100 mV s^{-1}.

3. Results and discussion

3.1. Pt deposition yield

UV–vis spectrophotometry analysis revealed that the yield for Pt particle deposition, defined as the weight percent of Pt deposited on the powder respect to the expected value, on the three carbon supports was different. Table 2 reports the Pt content for the three synthesised composites, as derived by UV–vis spectrophotometric analysis. Surface area of the different supports (Table 1) did not appear to be the discriminating factor affecting the yield of Pt deposition, which is better ascribed to the extremely different morphology and surface reactivity. The highly defective structure of SWNH, due to the presence of pentagonal and heptagonal rings of carbon atoms, which are responsible for the curvature in a graphene sheet, could determine the enhanced activity toward adsorption of the Pt precursor complexes, which in turn affects the Pt nuclei formation.

3.2. XRD analysis results

Fig. 1 reports the XRD patterns of the three Pt/C composites, showing the presence of the face-centred cubic structure typical of metallic platinum, represented by the crystalline planes: (1 1 1), (2 0 0), (2 2 0), (3 1 1). The position of the (0 0 2) reflection of graphite was different between the three carbon supports. In particular, in the case of carbon black the distance between the graphitic planes is larger than in the other two structures; in fact, the weak broad 0 0 2 peak is positioned at 2θ ~24.3° instead of about 26.3° expected for parent graphite. SWNH and MWNT presented two main components, one associated to a graphite-type structure and the other

Table 2
Pt wt% deposited on the three carbon supports and the yield of the deposition process.

	Pt deposited (wt%)	Deposition yield (%)
Pt/SWNH	13.5	67.5
Pt/MWNT	12.7	63.5
Pt/VU	8.4	42.0

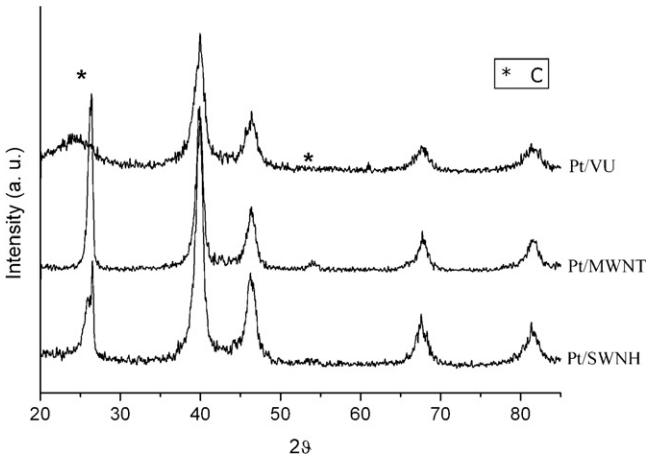

Fig. 1. X-Ray diffraction patterns of the three Pt/C composites.

associated to the peculiar structure of these nanostructures, as explained in [37] and [30], respectively.

Pt average crystallite size, *L*, can be obtained by Scherrer's equation [36], which relates *L* to the XRD peak broadening. The 220 reflection of Pt of these samples (Fig. 2) is suitable for Scherrer analysis because it does not present overlapping with reflections due to other phases. For identical deposition processes, the crystallite size of Pt changed with the carbon support (Table 3) and the smallest Pt particles deposited were those on Vulcan XC-72. Pt particle surface, *S*, was calculated assuming that the particles have a spherical shape [38] (Table 3).

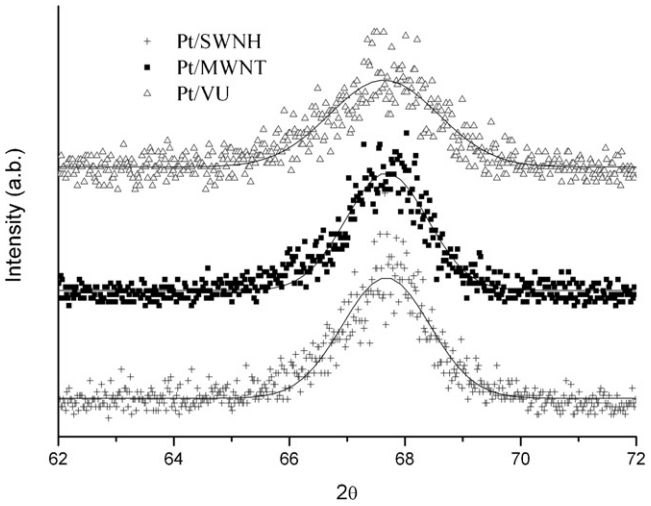

Fig. 2. 220 reflection of Pt crystals and curves resulted from fitting.

Table 3
Average particle size, surface area of catalyst and lattice parameters of Pt, for all the synthesised samples, evaluated from X-Ray Diffraction analysis.

Sample	L (nm)	S ($m^2\ g^{-1}$)	a (nm)
Pt/SWNH	6.15	45.6	0.3923
Pt/MWNT	6.49	43.2	0.3913
Pt/VU	4.83	58.1	0.3919
Pt/VU-COMM	2.12	131.9	0.3921

3.3. Electron microscopy observations

Figs. 3 and 4 show SEM and TEM micrographs of the three Pt/C composites, respectively, highlighting their morphological differences. The carbon black structure appears as a chain composed of quite-spherical elementary particles with diameter ranging from 20 to 50 nm. The surface of these primary particles is smooth. SWNH are similar to carbon blacks, but the surface of the primary particles is uneven, the roughness being generated by the "horns" protruding from the particles themselves. In the case of MWNT, finally, the nanotubes protrude from the particles. The electron microscope observations showed how the formation of aggregates of Pt particles depended on the carbon support. Fig. 3 shows the Pt particles deposited on SWNH, MWNT, and Vulcan, respectively. A larger amount of aggregates of Pt particles was found in SWNH and MWNT samples than in Vulcan sample. For the Pt/SWNH sample, the aggregate diameter was in the 50–100 nm range, while for the Pt/MWNT sample the diameter ranged from 20 to 50 nm. The aggregates observed were formed by small Pt particles (<4 nm). This result demonstrates the existence of single Pt particles and nanostructured aggregates of Pt particles. On the other hand, Pt deposited on Vulcan was not well dispersed: in fact, the sample exhibited some carbon primary particles not covered by Pt crystals (Fig. 3e and f).

TEM images show that the shapes of the Pt particles are dissimilar. While particles have a quite-spherical shape in the case of Pt deposited on Vulcan, particles deposited on MWNT and on SWNH seemed to have an elongated shape. Fig. 4d shows an HRTEM image of the aggregate of Pt particles. It is not clear yet if the particles coalesced or if they remained separated. The latter case, supported by

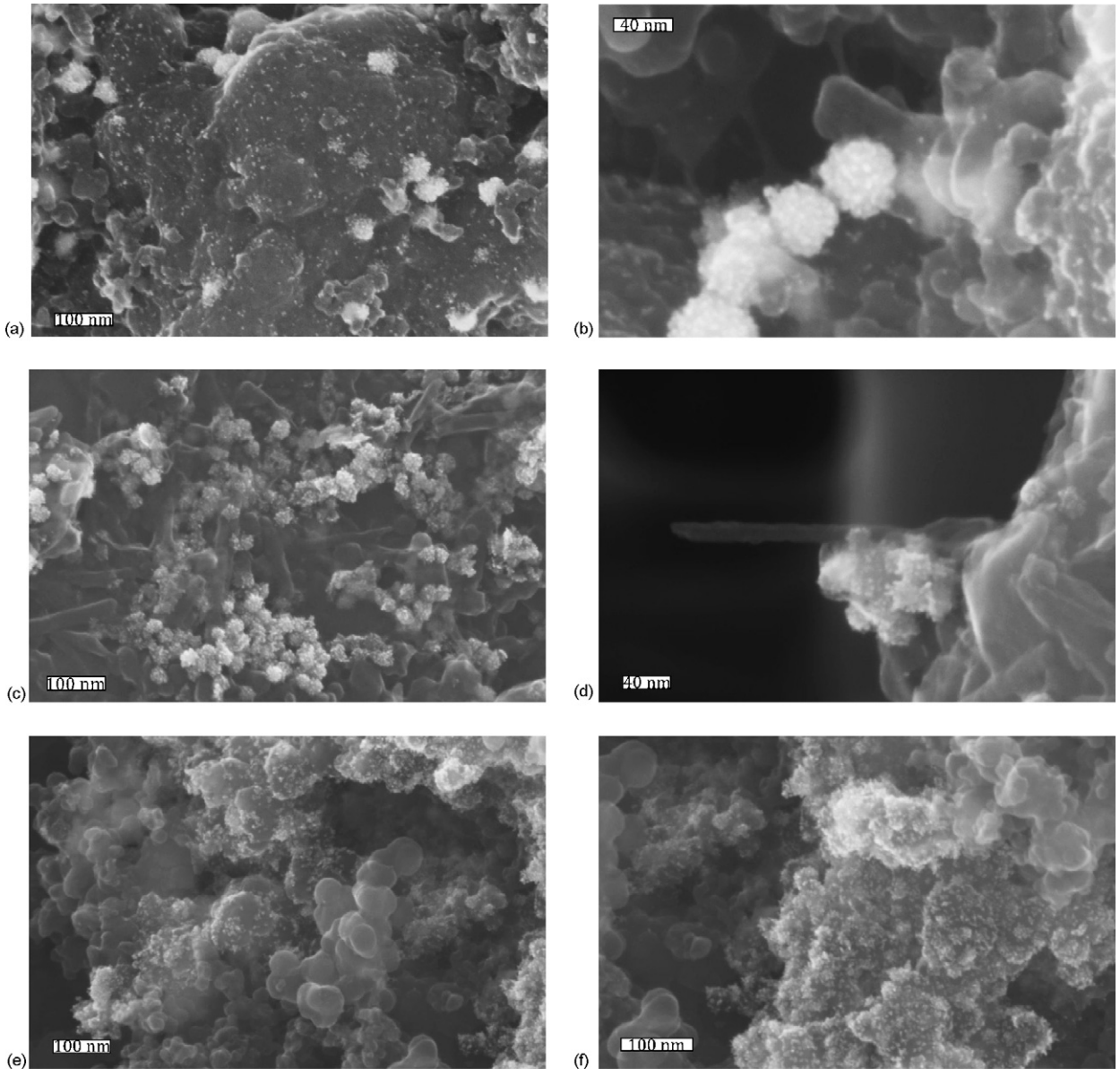

Fig. 3. Pt particles and aggregates deposited on: SWNH, (a) and (b); MWNT, (c) and (d); Vulcan XC-72, (e) and (f).

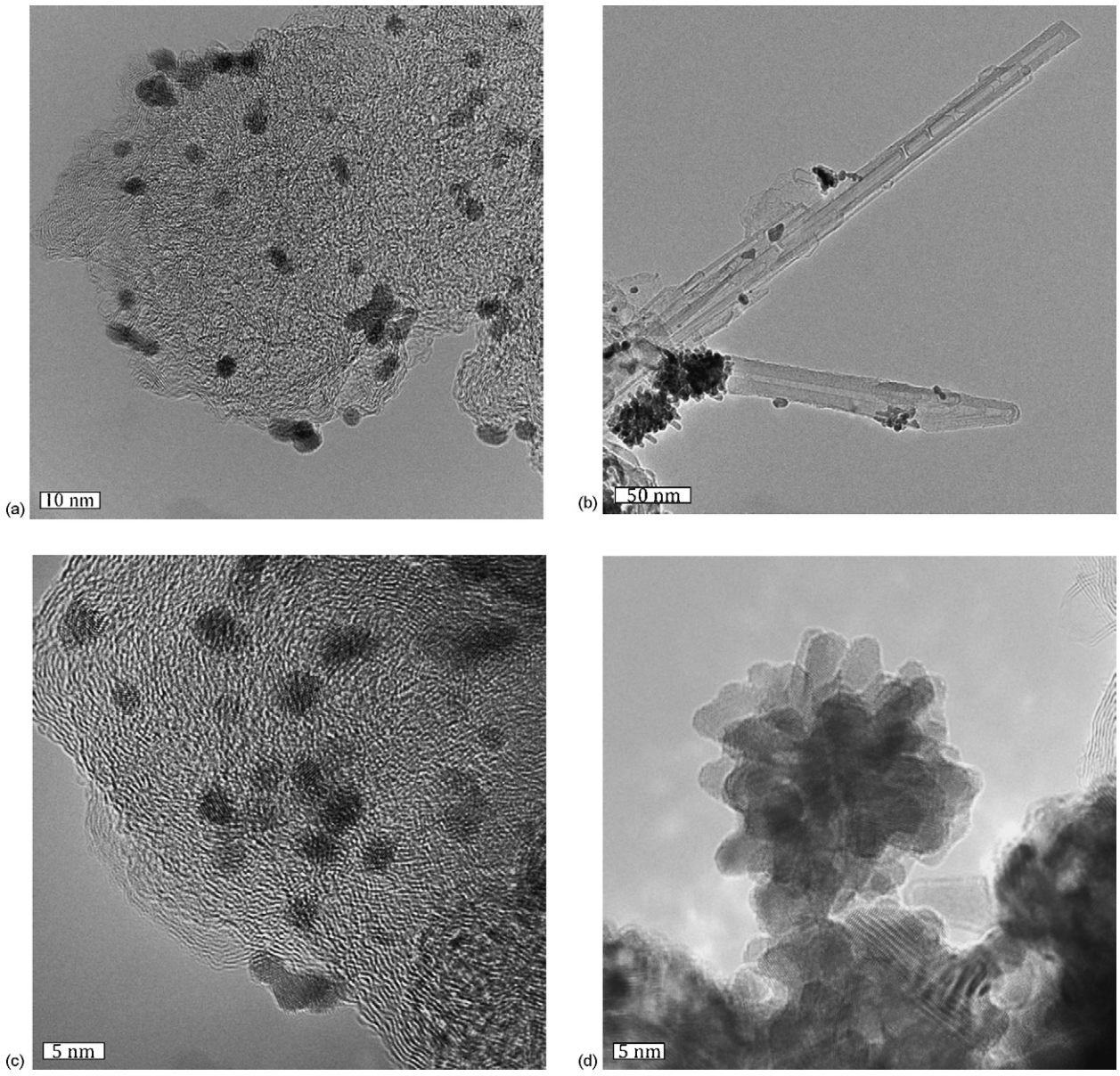

Fig. 4. TEM images of Pt/SWNH (a), Pt/MWNT (b) and Pt/VU (c) respectively. (d) is an HRTEM image of an aggregate of Pt particles found both on SWNH and on MWNT.

numerous TEM observations, seems to prevail. The aggregates (as in Fig. 4d) were found in larger quantity in the Pt/SWNH and Pt/MWNT samples. This finding shows that the carbon support has an important role in controlling the morphology of Pt particles deposited on its surface.

3.4. Cyclic voltammetry

The body of results, obtained by means of different techniques, demonstrated that the three Pt/C composites showed very different characteristics. Such characteristics may explain their different behaviour in cyclic voltammetry (CV) experiments.

The electrochemical active surface of the catalysts was evaluated by measuring the charge for hydrogen desorption [39–42]. Fig. 5 shows the potential sweeps on Pt/C electrodes, performed in 1 M H_2SO_4 solution at 30 °C. The potential region of interest is the one related to the hydrogen adsorption and desorption, at negative potentials. EAS values are reported in the third column of Table 4, where the Pt particle surface area measured by XRD is reported for sake of comparison (second column). There is a very good agreement between the active surface area evaluated by CV and XRD for the Pt/MWNT and Pt/VU samples, while the values obtained for the Pt/SWNH and Pt/VU-COMM samples are extremely discordant. The reason why these values are different is probably due to the differ-

Table 4
Electrochemical results for the four synthesised electrodes.

Sample	S ($m^2\ g^{-1}$) particle surface XRD	EAS before MOR ($m^2\ g^{-1}$)	EAS after MOR ($m^2\ g^{-1}$)	EAS loss (%)
Pt/SWNH	45.6	23.2	4.6	80.3
Pt/MWNT	43.2	41.7	39.0	6.6
Pt/VU	58.1	56.9	53.6	5.7
Pt/VU-COMM	131.9	23.7	7.9	66.9

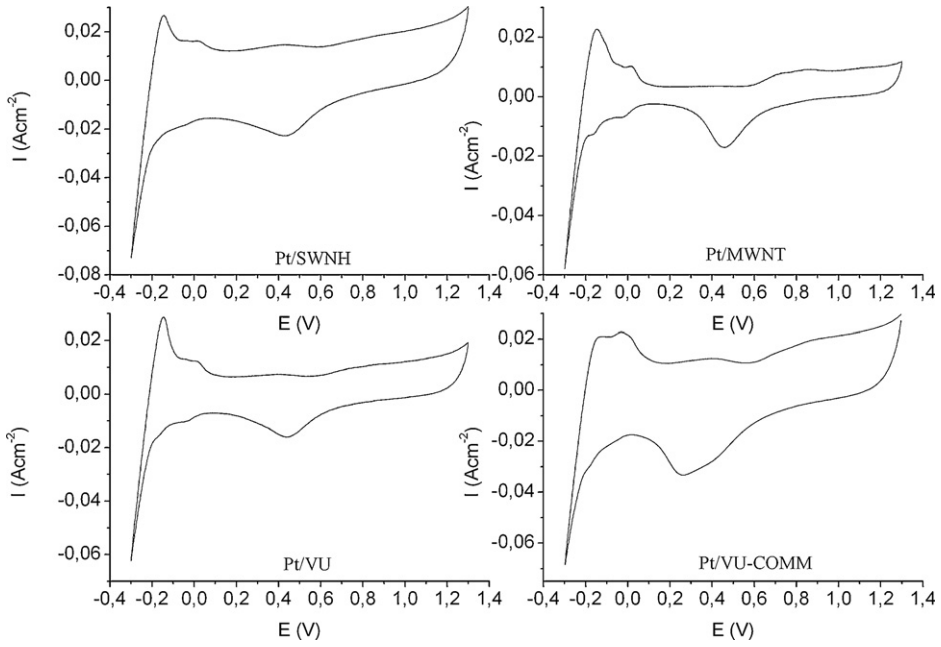

Fig. 5. Potential sweeps on Pt/C electrodes. 1 M H_2SO_4 solution at 30 °C (E vs SCE).

ent access of H^+ ions to the Pt surface in the four samples. The low EAS measured for the Pt/SWNH sample could be correlated with the presence of large agglomerates of Pt particles where Pt active sites are not exposed to hydrogen in the adsorption/desorption reactions, and consequently the charge associated to the hydrogen desorption was drastically reduced with respect to the other samples. The high Pt EAS and surface area of the Pt/VU sample could be substantially explained by the smaller Pt particle size and by a suitable contact between the reactants and the particles.

To simulate numerous cycles of methanol oxidation reaction, which takes place at the anode of a DMFC, 200 potential sweeps on Pt/C electrodes, in a 1 M H_2SO_4 solution added with 0.5 M CH_3OH at 30 °C, were carried out, and the results are shown in Fig. 6. The mass specific activity (MSA) of the Pt particles toward the methanol oxidation reaction was evaluated dividing the charge for methanol oxidation, corresponding to the area under the peak relative to methanol oxidation, by the Pt loading. Fig. 7 shows the MSA values calculated for 200 cycles. In the methanol oxidation reaction, the Pt/MWNT sample was more active and extremely stable, even after a large number of cycles, 200. The other electrodes showed quite the same behaviour. In these cases, though, MSA continued to decrease faster than for the Pt/MWNT electrode during the 200 cycles. It is worth to notice that the slope of the MSA vs cycle number plot for the four electrodes in the equilibrium region was different. The lower slope observed for the Pt/MWNT electrode demonstrated the sample long-term stability with respect to the ageing process.

To evaluate the reduction of electrochemical active surface of the Pt particles due to the methanol oxidation reaction, potential

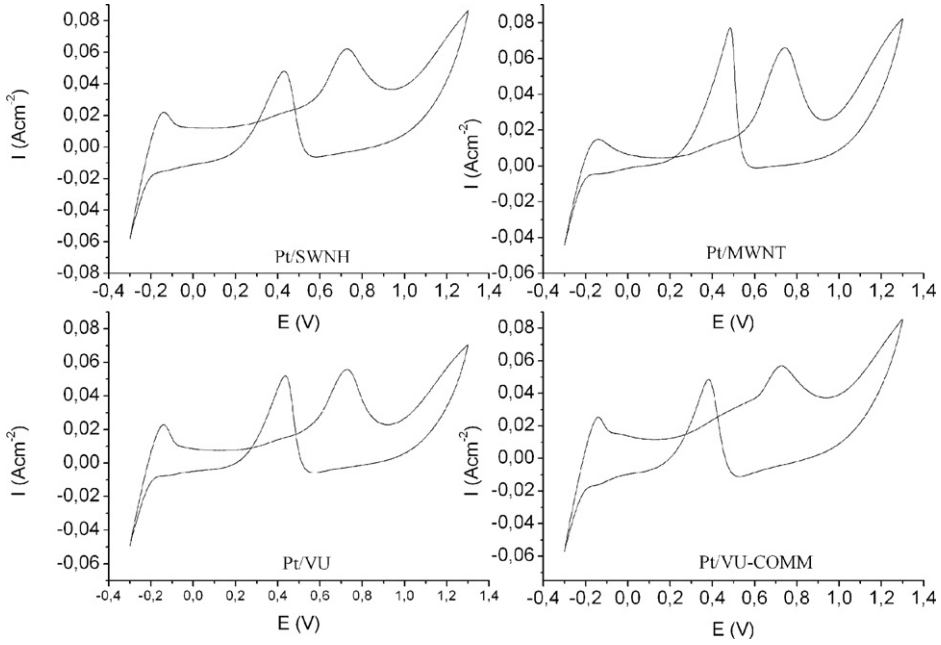

Fig. 6. Potential sweeps on Pt/C electrodes. 1 M H_2SO_4 solution + 0.5 M CH_3OH at 30 °C (E vs SCE).

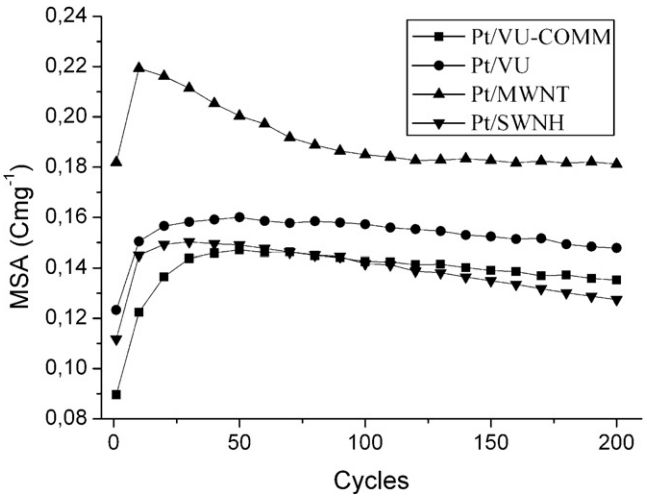

Fig. 7. Mass specific activity of the four Pt/C samples in function of the number of cycles of potential sweeps. 1 M H_2SO_4 solution + 0.5 M CH_3OH at 30 °C.

sweeps on Pt/C electrodes after MOR in 1 M H_2SO_4 at 30 °C were performed (Fig. 8). The values of EAS after MOR and EAS loss for the four electrodes are reported in the Table 4. While EAS values for the Pt/MWNT and PT/VU samples did not change significantly, the Pt losses for the Pt/VU-COMM and Pt/SWNH samples were 67 and 80%, respectively. Such extremely large EAS loss can be attributed either to materials leakage during potential sweeps or to Pt redistribution with suppression of active sites. The shape of the potential sweeps in the hydrogen region for the Pt/SWNH changed drastically (in comparison to Fig. 5), suggesting a redistribution of the Pt particles at atomic level with possible suppression of active sites. The shape of the peaks for this sample, in the hydrogen region, assumed the shape of the Pt/VU-COMM electrode peaks, in the same region. Thus, carbon support influences not only the characteristics of the Pt particles during the deposition process, but it also affects the redistribution of Pt particles during the potential sweeps.

3.5. Electron microscopy observations on electrodes after MOR

To better investigate the effect of the methanol oxidation reaction on the Pt particles, SEM observations at high magnification were carried out directly on the electrodes after a gentle drying treatment. Fig. 9 shows the SEM micrographs at low and high magnifications for all the electrodes after MOR. A comparison with the images reported in Fig. 3, shows that the potential sweeps in methanol solution caused the complete atomic redistribution of Pt particles, followed by the formation of large Pt particles of 10–30 nm in diameter. The particles shape was also changed. However, while in the Pt/SWNH, PT/VU, and Pt/VU-COMM electrodes the redistribution of Pt particles seemed to give the same results (similar particles in shape, smoothed surface, and diameter), in the case of the Pt/MWNT electrode it is possible to observe the presence of some larger particles, but with a nanostructured surface. These results could explain the better performance toward methanol oxidation reaction of the Pt/MWNT electrodes.

The redistribution of Pt atoms on the carbon surface might be explained by the different potential energy barrier for the different samples. In fact, the surface heterogeneity of the carbon support, which affects the position and the quantity of trapping sites for Pt atoms, changes drastically with the carbon substrate type. Morphological changes in Pt particles observed after potential sweeps are a function of the substrate, as reported before. The energy supplied during voltammetric cycles is large enough to extract the Pt atoms from the crystallites. Pt atoms diffuse on carbon surface due to the presence of charge gradients, and they are trapped in preferential sites depending on the potential energy. The same approach has been discussed by Flynn and Wanke [43] who considered the redistributing atoms, on thermal treated Pt/C composites, as a "two-dimensional" gas and they hypothesised that surface heterogeneities on the support could provide potential energy barriers for the migration of atoms. Their approach could be profitably applied to the current work. In this case it is not only important how much the surface heterogeneities could influence the diffusion of Pt atoms on carbon support surface, but in particular how, i.e. the effects in term of aggregate size and surface morphology on their electrochemical properties.

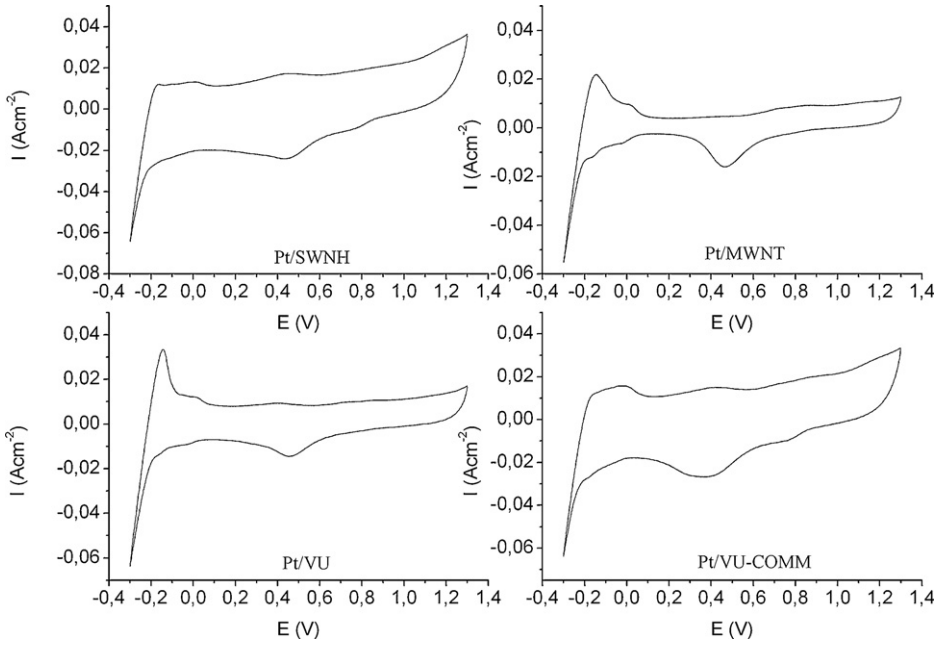

Fig. 8. Potential sweeps on Pt/C electrodes after MOR. 1 M H_2SO_4 solution at 30 °C (E vs SCE).

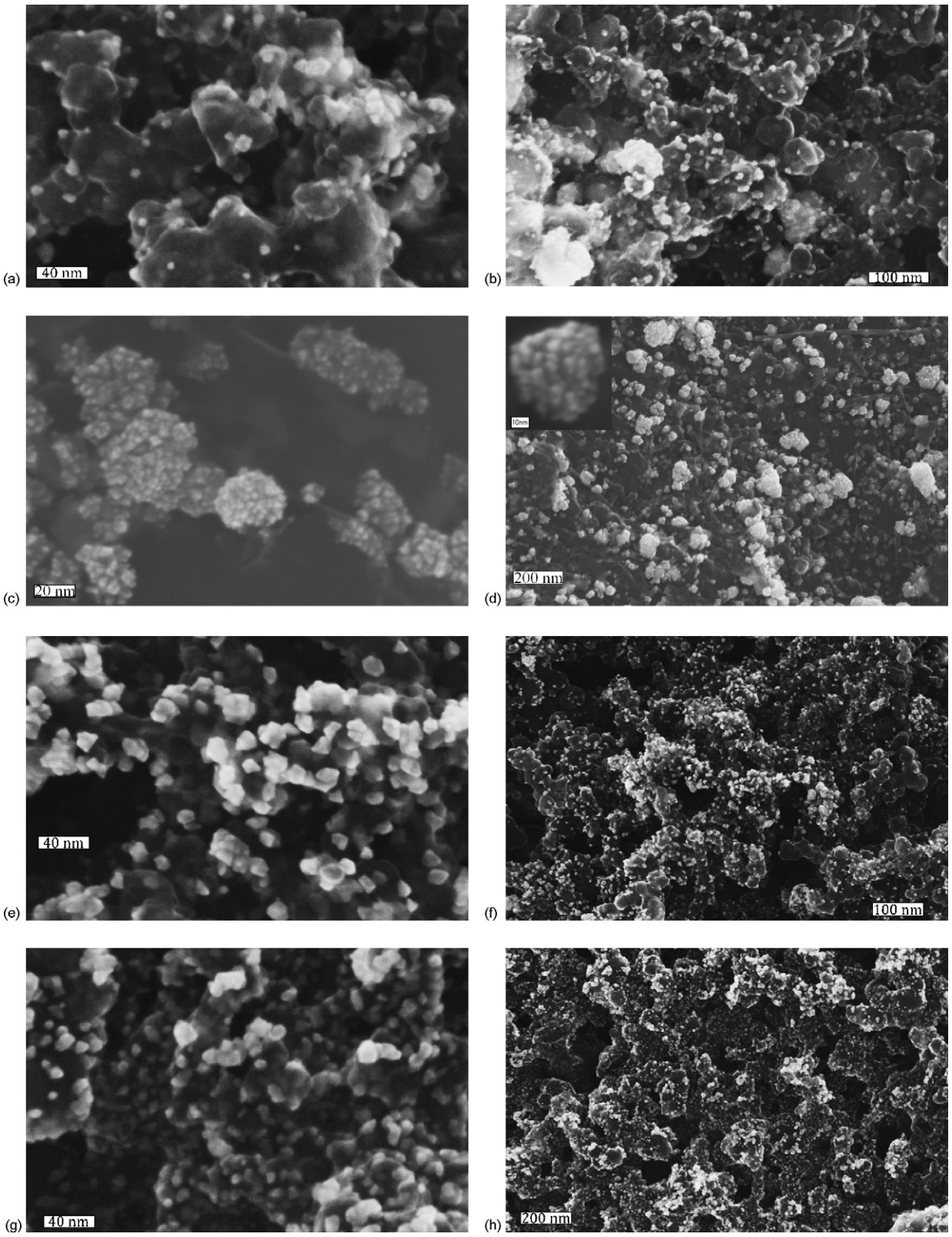

Fig. 9. SEM analyses on Pt/C electrodes after methanol oxidation reaction: Pt/SWNH, (a) and (b); Pt/MWNT, (c) and (d); Pt/VU, (e) and (f); Pt/VU-COMM, (g) and (h). In the inset of (d) a platinum particle found in the sample Pt/MWNT is showed at high magnification.

The SEM micrographs of the Pt particles after MOR cycles for the four electrodes investigated in this work, Fig. 9, show that Pt particles for Pt/SWNH, Pt/VU, and Pt/VU-COMM samples had quite the same shape and morphology, indicating a similar dimension order of the heterogeneities present in these carbon supports. The smooth surface of the carbon black and the jagged surface of the SWNH particles interacted quite in the same way with Pt diffusing atoms. It appears then that, at a fixed supplied energy, there

is a lower limit in the heterogeneity size beyond which Pt atoms aggregates in different shapes, as for the Pt/MWNT sample.

As shown in Fig. 7, the MSA, measured from methanol oxidation reaction cycles, changed during cycles allowing to reach an equilibrium state for Pt/C. Fig. 9 shows the configuration of the Pt aggregates and particles at this equilibrium state. This means that MOR continues even after 200 cycles for all the electrodes studied, at the equilibrium state, but the redistribution of Pt atoms (or platinum particles) on MWNT surface generated an electrode with better electrochemical performance and durability with respect to the other samples.

4. Conclusions

This work reports the deposition, by an impregnation process, of Pt particles on different carbon supports: multi-walled carbon nanotubes and single-walled carbon nanohorns, both prepared in our laboratory, and Vulcan XC-72 (VU) carbon black. A differential yield of deposition, which is not strictly related to the surface area of the carbon support, and particle dimension were observed. SWNH showed the higher surface chemical activity toward Pt deposition.

SEM and TEM observations showed how carbon supports seem to influence the structure of the deposited Pt particles and their aggregation.

Different configurations of Pt particles and aggregates lead to different electrochemical results. Pt/VU showed the larger value of EAS. Our results demonstrated that the mass specific activity for the methanol oxidation reaction of Pt/MWNT composite was larger than those of Pt/SWNH and PT/VU composites.

The redistribution of Pt particles followed by the formation of large Pt particles of 10–30 nm in diameter was observed during methanol oxidation reaction. For the Pt/SWNH, PT/VU, and Pt/VU-COMM electrodes, the Pt particle redistribution seems to give the same results, which are similar particles in shape, smoothed surface, and diameter, while for the Pt/MWNT electrode some larger particles were observed, with a nanostructured surface. Diffusion of Pt atoms on carbon surface was used to explain the formation of Pt aggregates.

This work demonstrated how different nanocarbon supports lead to different characteristics of the deposited Pt particles and to a different redistribution of Pt particles during cycling.

The use of new carbon nanostructures, with respect to “blacks”, could enhance the performance of the electrode in fuel cells taking advantage of the specific interaction between Pt and MWNT or SWNH.

Acknowledgements

We thank Dr D. Marani for helpful discussions and Cadia D’Ottavi for her technical assistance. The financial support of the Italian Ministry for Foreign Affairs (Italy-Quebec Joint Lab for Advanced Nanostructured Materials for Energy, Catalysis and Biomedical Applications) is gratefully acknowledged.

The financial support of the Italian Ministry of Research through the project TEPSI is gratefully acknowledged.

References

[1] N.A. Alonso-Vante, H. Tributsch, Nature 323 (1986) 431–432.
[2] S. Mukerjee, S. Srinivasan, J. Electroanal. Chem. 357 (1993) 201–224.
[3] R. Bashyam, P. Zelenay, Nature 443 (2006) 63–66.
[4] T. Kawaguchi, Y. Rachi, W. Sugimoto, Y. Murakami, Y. Takasu, J. Appl. Electrochem. 36 (2006) 1117–1125.
[5] A.S. Aricò, Z. Poltarzewski, H. Kim, A. Morana, N. Giordano, V. Antonucci, J. Power Sources 55 (1995) 159–166.
[6] A. Pebler, J. Electrochem. Soc. 133 (1986) 9–17.
[7] M. Carmo, V.A. Paganin, J.M. Rosolen, E.R. Gonzalez, J. Power Sources 142 (2005) 169–176.
[8] P. Ehrburger, O.P. Mahajan, P.L. Walker Jr., J. Catal. 43 (1976) 61–67.
[9] P. Ehrburger, P.L. Walker Jr., J. Catal. 55 (1978) 63–70.
[10] R.J. Madix, J. Benziger, Ann. Rev. Phys. Chem. 29 (1978) 285–306.
[11] A. Norton Haner, P.N. Ross, J. Phys. Chem. 95 (1991) 3740–3746.
[12] E. Herrero, K. Franaszczuk, A. Wieckowski, J. Phys. Chem. 98 (1994) 5074–5083.
[13] E. Herrero, W. Chrzanowski, A. Wieckowski, J. Phys. Chem. 99 (1995) 10423–10424.
[14] S. Iijima, Nature 354 (1991) 56–58.
[15] K. Lee, J. Zhang, H. Wang, D. Wilkinson, J. Appl. Electrochem. 60 (2006) 507–522.
[16] N. Jha, A.L.M. Reddy, M.M. Shaijumon, N. Rajalakshmib, S. Ramaprabhua, Int. J. Hydrogen Energy 33 (2008) 427–433.
[17] A. Thess, R. Lee, P. Nikolaev, H. Dai, P. Petit, J. Robet, C. Xu, Y.H. Lee, S.G. Kim, A. Rinzler, D.T. Colbert, G. Scuseria, D. Tomanek, J.E. Fischer, R. Smalley, Science 273 (1996) 483–487.
[18] D. Pantea, H. Darmstadt, S. Kaliaguine, L. Summchen, C. Roy, Carbon 39 (2001) 1147–1158.
[19] W. Li, C. Liang, W. Zhou, J. Qiu, Z. Zhou, G. Sun, Q. Xin, J. Phys. Chem. B 107 (2003) 6292–6299.
[20] L. Li, Y. Xing, J. Electrochem. Soc. 153 (2006) A1823–A1828.
[21] T. Yoshitake, Y. Shimakawa, S. Kuroshima, H. Kimura, T. Ichihashi, Y. Kubo, D. Kasuya, K. Takahashi, F. Kokai, M. Yudasaka, S. Iijima, Physica B 323 (2002) 124–126.
[22] S. Iijima, M. Yudasaka, R. Yamada, S. Bandow, K. Suenaga, F. Kokai, K. Takahashi, Chem. Phys. Lett. 309 (1999) 165–170.
[23] N.M. Rodriguez, M.-S. Kim, R.T.K. Baker, J. Phys. Chem. 98 (1994) 13108–13111.
[24] F. Salman, C. Park, R.T.K. Baker, Catal. Today 53 (1999) 385–394.
[25] A. Chambers, T. Nemes, N.M. Rodriguez, R.T.K. Baker, J. Phys. Chem. B 102 (1998) 2251–2258.
[26] C. Park, R.T.K. Baker, J. Phys. Chem. B 102 (1998) 5168–5177.
[27] C. Park, R.T.K. Baker, J. Phys. Chem. B 103 (1999) 2453–2459.
[28] I.-S. Park, K.-W. Park, J.-H. Choi, C.R. Park, Y.-E. Sung, Carbon 45 (2007) 28–33.
[29] C:A. Bessel, K. Laubernds, N.M. Rodriguez, R.T.K. Baker, J. Phys. Chem. B 105 (2001) 1115–1118.
[30] V. Contini, R. Mancini, R. Marazzi, D. Mirabile Gattia, M. Vittori Antisari, Phil. Mag. 87 (2007) 1123–1137.
[31] D. Mirabile Gattia, M. Vittori Antisari, R. Marazzi, Nanotechnology 18 (2007) 255604–255611.
[32] D. Bera, G. Johnston, H. Heirich, S. Seal, Nanotechnology 17 (2006) 1722–1730.
[33] R. Yuge, T. Ichihashi, Y. Shimakawa, Y. Kubo, M. Yudasaka, S. Iijima, Adv. Mater. 16 (2004) 1420–1423.
[34] H.E. van Dam, H. van Bekkum, J. Catal. 131 (1991) 335–349.
[35] M. Balcerzak, E. Swiecicka, E. Balukiewicz, Talanta 48 (1999) 39–47.
[36] H.P. Klug, L.E. Alexander, X-ray Diffraction Procedures, Jonh Wiley, New York, 1954, p491-538.
[37] S. Bandow, F. Kokai, K. Takahashi, M. Yudasaka, L.C. Qin, S. Iijima, Chem. Phys. Lett. 321 (2000) 514–519.
[38] O. Stonehart, J. Appl. Electrochem. 22 (1992) 995–1001.
[39] T. Biegler, D.A.J. Rand, R. Woods, J. Electroanal. Chem. 29 (1971) 269–277.
[40] R. Woods, J. Electroanal. Chem. 49 (1974) 217–226.
[41] M. Watanabe, K. Makita, H. Usami, S. Motoo, J. Electroanal. Chem. 197 (1986) 195–208.
[42] A. Pozio, M. De Francesco, A. Cemmi, F. Cardellini, L. Giorgi, J. Power Sources 105 (2002) 13–19.
[43] P.C. Flynn, S.E. Wanke, J. Catal. 34 (1974) 390–399.